Theoretical and Applied Climatology (2024) 155:1321–1341
https://doi.org/10.1007/s00704-023-04692-x

RESEARCH

Extreme warm and cold waves derived from multiple high-resolution gridded datasets in Egypt

Hassan Aboelkhair[1] · Mostafa Morsy[2]

Received: 13 March 2023 / Accepted: 27 September 2023 / Published online: 11 October 2023

Abstract
The primary purpose of this study is to interpret the variability of extreme warm (Tmax) and cold (Tmin) events over Egypt from 1981 to 2020 using three gridded datasets that evaluated against the observations at 24 in situ stations using robust statistical procedures. These high-resolution gridded datasets are well-matched with the observed data. Furthermore, the monthly maximum of daily Tmax (TXx) and Tmin (TNx) and the monthly minimum of daily Tmax (TXn) and Tmin (TNn) climate indices are used to investigate the variability of extremes over Egypt. It is found that the TXx increased gradually throughout the study period and the Mann–Kendall rank correlation (Tau) is mostly positive in the first and last decades, with the coefficient of variation (COV) ranges from 1 to 5. Also, the lowest TXn values are detected in the first two decades with decadal anomaly ranging from − 2 to + 2, and it has positive Tau values during all decades with COV ranges from 2 to 20. The TNx increased southward, and its decadal anomaly increased gradually over time. The significant positive Tau of TNx is found in the first and last decades, and its COV ranges from 1 to 8. Moreover, the TNn is increased during the study period, and its anomaly is less than + 0.5 °C in the first decade and exceeds + 2 °C in the fourth decade. The significant positive (negative) Tau for TNn appeared during the third (fourth) decade, while its COV ranged from 1 to 12. Finally, the COV and Tau of all indices are often negatively correlated (> − 0.5).

1 Introduction

Most developing countries, like Egypt, suffer from a scarcity of meteorological weather stations over space and time (El Kenawy et al. 2019a). Also, the available observations are uncertain due to the proximity of most weather stations to urban settlements, within airports, and on coasts (Peterson et al. 1998). As a result, more than the available observations are insufficient to study and understand the spatio-temporal changes of most atmospheric parameters; thus, reanalysis datasets are often used instead of observational data to overcome such limitations (El Kenawy et al. 2019b). Many operational centers worldwide have produced, developed, and updated various reanalysis datasets over the last few decades that include a variety of observations. They are freely available (e.g., European Centre for Medium-Range Weather Forecasts (ECMWF), National Centers for Environmental Prediction (NCEP), and the National Aeronautics and Space Administration (NASA)). Accordingly, many studies and applications concerned with climate extremes have used such datasets in different regions around the world, such as ECMWF/ERA-Interim over Egypt (Morsy and El Afandi 2021), ERA-40, JRA-55, and 20CR over China (Zhao et al. 2020), Observational-Reanalysis Hybrid OR above East of Africa (Gebrechorkos et al. 2019), and NASA POWER in Mediterranean region (Rodrigues and Braga 2021). The reanalysis from the fifth-generation ECMWF/ERA5 has decreased climatological temperature biases and enhanced the depiction of inter-annual variability over East Africa (Gleixner et al. 2020). NASA Prediction of Worldwide Energy Resources (NASA/POWER) dataset provided a reasonable performance for the near-surface parameters (except for relative humidity) against in situ observations, and it can be used in case of missing or unavailable observations, particularly for maximum and minimum temperature over Egypt

✉ Hassan Aboelkhair
aboelkhair@art.tanta.edu.eg

Mostafa Morsy
mostafa_morsy@azhar.edu.eg

[1] Department of Geography and Geographical Information Systems, Faculty of Arts, Tanta University, Tanta 31527, Gharbiya, Egypt

[2] Astronomy and Meteorology Department, Faculty of Science, Al-Azhar University, Cairo 11884, Egypt

(Aboelkhair et al. 2019). Furthermore, the Climate Forecast System Reanalysis (NCEP/CFSR) dataset for temperature products may perform well in monthly streamflow and evapotranspiration simulations, making it a viable alternative data source for hydrological simulations in certain gauge-deficient regions (Zhang et al. 2020).

Severe weather occurrences have increased in frequency and intensity, resulting in more worldwide catastrophes that significantly affect society and the economy (Zhou et al. 2020; Chikabvumbwa et al. 2022). Globally, extreme warm events increased, and extreme cold events decreased, especially in the Loess Plateau (China), where the trend amplitudes of cold extremes were higher than those of warm extremes (Sun et al. 2016). Also, the frequency of severe hot and cold weather occurrences in Nigeria has increased significantly, and the cold weather events have decreased, where the most notable trends in warm and cold nights are in Guinea and the Sahel regions (Abatan et al. 2016). Furthermore, as the earth warms, cold extremes will decrease while warm extremes increase, making the vulnerability of cold extremes to climate change more remarkable than warm extremes (Wang et al. 2017). Finally, the evaluating of the different available reanalysis datasets in measuring extreme climatology and long-term trends in extreme climate provides valuable information. However, investigating reanalysis datasets in quantifying the temperature extremes (warm and cold) under climate change conditions still needs comprehensive studies. Where most of the previous studies focused on study the changes of heatwave indices and aspects over Egypt (Morsy and El Afandi 2021), Arabian Peninsula (Almazroui et al. 2017), Middle East and North Africa region (Driouech et al. 2020), and Eastern Mediterranean and the Middle East (Lelieveld et al. 2012; Zittis et al. 2016). Therefore, this study aims the following:

1- To identify the performance of multiple gridded reanalysis datasets (ERA5, CFSR, and POWER) for the spatio-temporal distribution of maximum and minimum temperatures during four consecutive decades (1981–2020) over Egypt.
2- To assess the spatio-temporal suitability of these gridded reanalysis datasets to explain the extreme events and reproduce the changes in warm and cold extreme temperatures.
3- To investigate and interpret the decadal and spatial variability, anomaly, and trend for different maximum and minimum temperature indices during the climate period from 1981 to 2020 over Egypt.

2 Study area

Egypt is located in the northeastern part of Africa, with its borders roughly ranging from 22° to 32° N and from 25° and 38° E with a total area of about 1.01 million km^2. The Mediterranean Sea bordered it to the north, while the Red Sea bound it to the east (Fig. 1). From the climatological point of view, Egypt has a semi-desert climate in the south and a Mediterranean climate in the north. During the summer, it is hot and dry, while it is mild and rainy in the winter. According to the Köppen climatic classification, Egypt has a hot desert climate. Consequently, the weather is often dry throughout the year (Nashwan 2019).

3 Dataset and methodology

3.1 Data acquisition

To achieve the main objectives of this study, near-surface (2-m) maximum (Tmax) and minimum (Tmin) temperatures are downloaded from four different data sources. These datasets include observational data at 24 ground-based weather stations covering the different Egyptian climatic zones (Fig. 1), and three high resolution gridded datasets, as described in Table 1. The observed dataset is obtained from the Global Surface Summary of the Day (GSOD) on the NOAA National Centers for Environmental Information (NCEI) website (https://www.ncei.noaa.gov/maps/daily/). The observed data is used to evaluate and investigate the accuracy of the other three gridded reanalysis datasets and to assess their performance and suitability for simulating temperature extremes. The three acquired reanalysis datasets are ECMWF/ERA5 (https://cds.climate.copernicus.eu/), NASA/POWER (https://power.larc.nasa.gov/data-access-viewer/), and NCEP (CFSR: https://rda.ucar.edu/datasets/ds093.0/; CFSv2: https://rda.ucar.edu/datasets/ds094.0/).

The obtained hourly ERA5 and 6-h NCEP datasets are converted to daily datasets using the Climate Data Operator (CDO) to obtain a temporal resolution compatible with the observed data and the NASA /POWER dataset.

3.2 Statistical evaluation of gridded reanalysis datasets

Several robust statistical procedures are applied to measure the goodness of fit and accuracy of the ERA5, CFSR, and POWER datasets for Tmax and Tmin estimates and capture their extremes (warm and cold) against observation. The used statistical metrics are as follows:

3.2.1 Coefficient of determination (R2)

Coefficient of determination (R^2) is a method of calculating the accuracy of datasets by quantifying the variance in observed data, which is explained by the variation in the

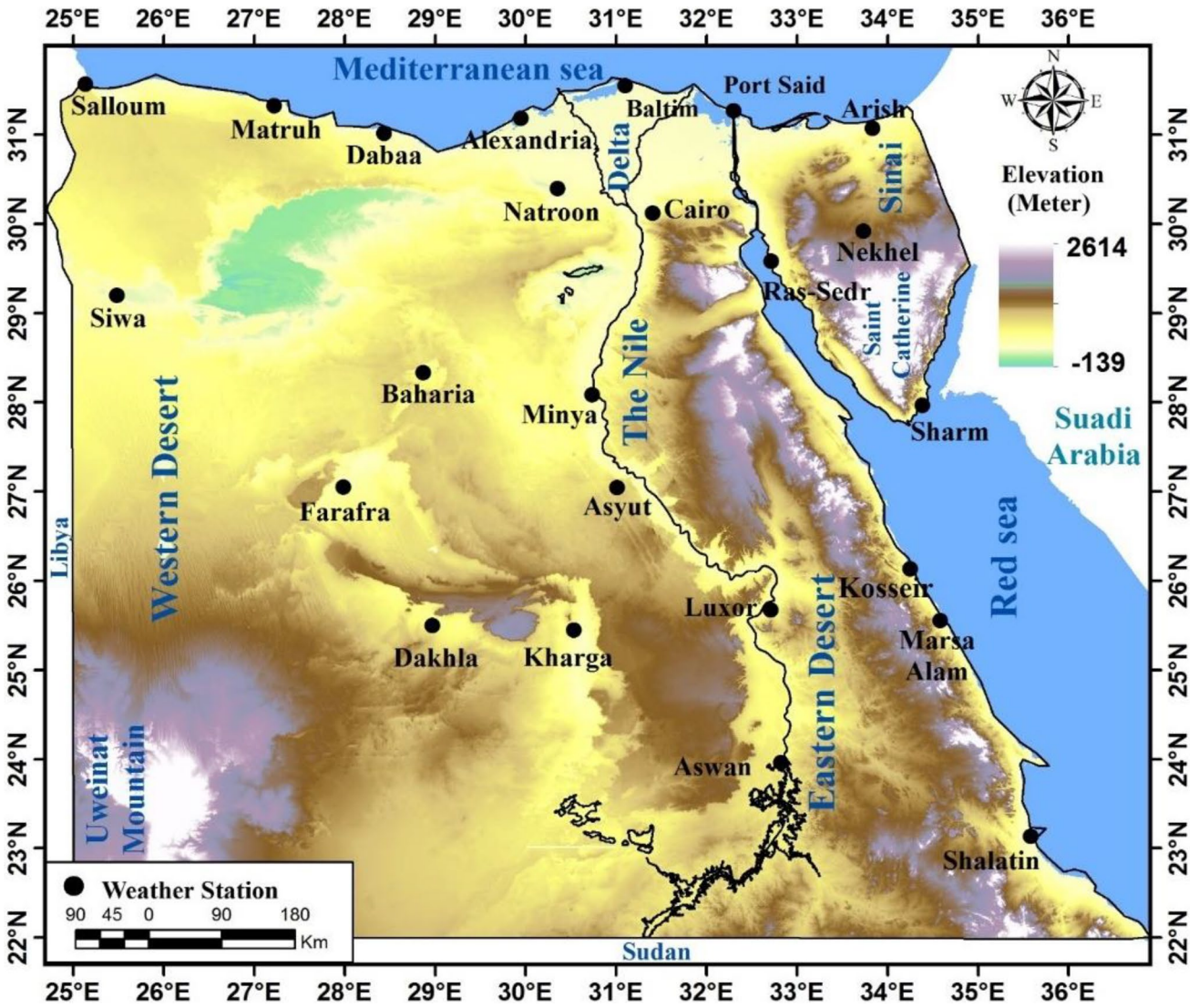

Fig. 1 The geographical distribution and elevation of the selected weather stations in Egypt

Table 1 The main characteristics of the used observation and reanalysis datasets

Dataset	Horizontal resolution	Temporal resolution	Period	Reference
Observations	Stations	Daily	01/01/1981–31/12/2020	Lott et al. 2001
ECMWF/ERA5	0.25°×0.25°	Hourly		Hersbach et al. 2018
NASA/POWER	0.5°×0.5°	Daily		Duarte and Sentelhas 2020
NCEP/CFSR	0.5°×0.5°	6 hours	01/01/1981–31/12/2010	Saha et al. 2010
NCEP/CFSv2			01/01/2011–31/12/2020	Saha et al. 2011

estimated data from gridded datasets. It ranges from 0 to 1, where the highest values (closer to 1) show less error fluctuation and a better match, and values greater than 0.5 are acceptable (Pineiro et al. 2008; Moriasi et al. 2007).

$$R^2 = 1 - \frac{\sum_{i=1}^{n} \left(O_i - R_i\right)^2}{\sum_{i=1}^{n} \left(O_i - O_a\right)^2} \quad (1)$$

where O_i, O_a, and R_i are the observed, observed average, and reanalysis values, and n is the number of accessible observations.

3.2.2 Willmott index of agreement (WI)

Willmott index of agreement (WI) is the standardized measure of gridded reanalysis datasets error ranging from 0 to 1.

The number of 1 represents the complete agreement, and the value of 0 shows no agreement at all (Willmott 1981; Abba et al. 2020).

$$\mathrm{WI} = 1 - \frac{\sum_{i=1}^{n} \left(O_i - R_i\right)^2}{\sum_{i=1}^{n} \left(\left|R_i - O_a\right| - \left|O_i - O_a\right|\right)^2} \tag{2}$$

3.2.3 Mean bias error (MBE)

Mean bias error (MBE) is a measure that shows if the gridded reanalysis dataset is overestimated or underestimated by comparing it with the actual observations in terms of systematic error (Willmott and Matsuura 2005; Singh et al. 2013).

$$\mathrm{MBE} = \frac{\sum_{i=1}^{n} (R_i - O_i)}{n} \tag{3}$$

3.2.4 Root mean square error (RMSE)

Root mean square error (RMSE) is a measure of the mean standard deviation of gridded reanalysis datasets compared the observed values (Gauch et al. 2003; Bai et al. 2010).

$$\mathrm{RMSE} = \sqrt{\frac{\sum_{i=1}^{n} \left(R_i - O_i\right)^2}{n}} \tag{4}$$

3.2.5 Mean absolute error (MAE)

Mean absolute error (MAE) gives equal weight to all individual deviations for the gridded reanalysis datasets compared to the actual observations throughout the test sample (Chai and Draxler 2014; Willmott and Matsuura 2005)

$$\mathrm{MAE} = \frac{1}{n} \times \sum_{i=1}^{n} \left|O_i - R_i\right| \tag{5}$$

3.2.6 Mean percentage error (MPE %)

Mean percentage error (MPE %), a positive MPE value indicates that the gridded reanalysis dataset values are underestimated on average. In contrast, a negative value indicates that the gridded reanalysis dataset values are overestimated (Ouda et al. 2015).

$$\mathrm{MPE} = \frac{\sum_{i=1}^{n} \left(\frac{(O_i - R_i)}{O_i} \times 100\right)}{n} \tag{6}$$

3.3 Temperature indices, variability, and Mann–Kendall test

The climate data operator (CDO) tool is used to compute several indices that describe the changes in temperature extremes including monthly maximum value of daily Tmax (TXx °C), monthly minimum value of daily Tmax (TXn °C), monthly maximum value of daily Tmin (TNx °C), monthly minimum value of daily Tmin (TNn °C), and the coefficient of variation (COV) for these indices (TXx, TXn, TNx, and TNn). Also, the Grid Analysis and Display System (GrADS) software is used to calculate decadal average and anomaly of TXx, TXn, TNx, and TNn. Finally, the modified version of non-parametric Mann–Kendall test package (modifiedmk) in R software (Patakamuri et al. 2020) is used to perform the Mann–Kendall trend test of Pre-Whitened (pwmk) time series data in the presence of serial correlation using Yue and Wang (2002) approach. The pwmk test is employed to assess the existence of monotonic increasing or decreasing trends and the significant serial correlation (Tau) in the computed indices (TXx, TXn, TNx, and TNn). The performed sequential steps for Tau rank correlation are documented by Kendall (1970), where Kendall's Tau varies between − 1 for decreasing trend and + 1 for increasing trend.

4 Results and discussion

4.1 Statistical evaluation

The statistical metrics of R^2, WI, RMSE, MAE, MBE, and MPE are used to evaluate the daily Tmax (°C) and Tmin (°C) values from ERA5, CFSR, and POWER datasets against the observed values at the selected 24 metrological stations.

Figure 2 shows the geostatistical and spatial distribution of R^2, MBE, and RMSE between the estimated Tmax (°C) and Tmin (°C) values from the three gridded reanalysis datasets (ERA5, CFSR, and POWER) and observed values. To identify the goodness of fit and accuracy of the selected three datasets, the proportional symbol circle maps for R^2, MBE, and RMSE as geostatistical and spatial distribution maps covering all stations over Egypt are created and performed using ArcGIS Pro2.8.0 software.

As shown in Fig. 2a and b, both Tmax (°C) and Tmin (°C) have R^2 higher than 0.80, suggesting that more than 80% of the observed values are explained or estimated by the three gridded reanalysis dataset (ERA5, CFSR, and POWER). R^2 value for Tmax ranges from 0.93 to 0.98 °C in ERA5, from 0.90 to 0.98 °C in POWER, and from 0.89 to 0.97 °C in CFSR, while for Tmin, it ranges from 0.88 to 0.96 °C in ERA5, from 0.86 to 0.96 °C in POWER, and from 0.83

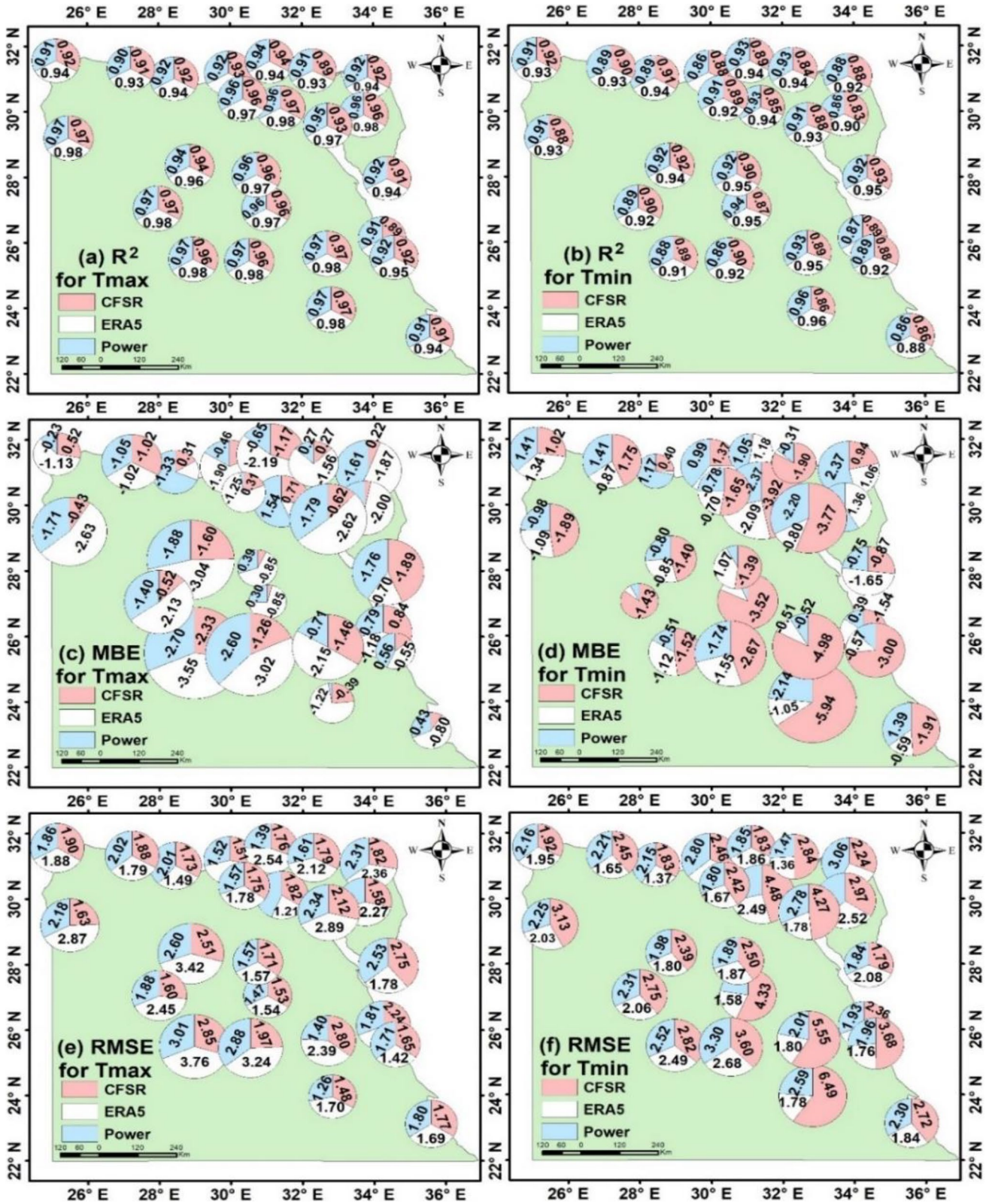

Fig. 2 Geostatistical and spatial distribution of Tmax (left panel) and Tmin (right panel) evaluation

to 0.93 °C in CFSR. These results indicate that the ERA5 dataset can further explain the observed values of Tmax and Tmin followed by POWER and CFSR. As shown in Fig. 2c, Dakhla, Kharga, and Bahria stations from the three gridded datasets have the highest MBE while Shalateen, Aswan, Asyut, and Minya stations have the lowest MBE for the Tmax. For Tmin (Fig. 2d), the highest MBE values from the three gridded datasets for Tmin are found at Cairo, Aswan, and Ras Sidr while the lowest MBE values are found at Farafra, Dabaa, and Minya. On the other hand, the geospatial distribution of RMSE from the three gridded datasets for Tmax and Tmin are shown in Fig. 2 e and f respectively. The highest RMSE values for Tmax are detected at Dakhla, Kharga, and Bahariya stations, and the lowest RMSE values are found at Shalateen, Aswan, Asyut, and Minya stations. Additionally, the highest RMSE values are found at Cairo, Aswan, and Ras Sidr, while the lowest RMSE values are found at Farafra, Dabaa, and Minya. It is also noticed that the geospatial distribution and values of RMSE closely match the geospatial distribution and values of MBE.

Also, WI, MAE, and MPE (not shown) are also utilized to assess the suitability and accuracy of the three gridded datasets. The WI values vary from 0.94 to 0.99 °C in the three gridded datasets for Tmax, while for Tmin, it ranges from 0.94 to 0.99 °C in the three gridded datasets except at Aswan, Cairo, Luxor, Marsa Alam, and Ras Sidr in the CFSR. Regarding MAE values for Tmax from ERA5, POWER, and CFSR are 3.58, 2.75, and 2.44 °C respectively, while its values for Tmin are 3.86, 2.74, and 2.23 °C for CFSR, POWER, and ERA5 respectively. Furthermore, the maximum MPE for Tmax is 8% in CFSR, 8.8% in POWER, and 11.68% in ERA5, while the maximum MPE for Tmin is 13.7% in ERA5, 14.5% in POWER, and 15% in CFSR. These results show that the three gridded datasets have goodness of fit, considerable agreement, and accurate estimation for Tmax and Tmin compared to the observed data along the study climate period (1981–2020) over Egypt.

4.2 Investigation of extremes

Due to the noticed slight differences in the accuracy of the three gridded datasets for estimating Tmax and Tmin values, their performance to simulate and capture the extreme warm and cold temperatures should be investigated to be used appropriately in the discussion and analysis of extremes.

Table 2 shows the differences for the highest Tmax values (heat wave) between the observed and estimated values from the three grid datasets at five stations (Aswan, Asyut, Cairo, Arish, and Matruh) in Egypt. Nine Tmax extreme events (cases) were detected throughout the study period (1981–2020) that agreed to occur at all stations, including five in June, three in July, and one in August. These nine events are selected as each event has no less than 3 consecutive days with Tmax greater than or equal to 30 °C at the five stations. For extreme warm of Tmax, the highest positive difference is 3.95 °C at Cairo in CFSR and the lowest positive difference is 0.09 °C at Aswan in ERA5, while the highest negative difference is − 3.91 °C at Arish in POWER, and the lowest negative difference is − 0.01 °C at Cairo in POWER.

Table 3 shows the differences for the lowest Tmin (cold wave) between the observed and estimated values from the three grid datasets at the same five stations in Egypt. It is noticed that there are 12 extreme cold events that have no less than 3 consecutive days with Tmin below 10 °C during the study period (1981–2020) including ten cases in January and two in February. For the extreme cold of Tmin, the CFSR in Arish station has the greatest positive difference (3.98 °C), and the CFSR in Cairo has the lowest positive difference (0.87 °C), while the CFSR in Aswan has the greatest negative difference (− 3.93 °C) and the POWER in Matruh has the lowest negative difference (− 0.20 °C).

For both Tmax and Tmin, the maximum positive and negative differences (errors) range from − 4 to 4 °C, revealing that the three gridded datasets can be properly used to discuss and analyze extreme warm and cold temperatures.

4.3 Extreme temperature variability

The decadal average, anomaly, variability, and trend of extreme Tmax indices (TXx, TNx) and extreme Tmin indices (TXn, TNn) computed from the three gridded datasets (CFSR, ERA5, and POWER) are discussed and analyzed in this section.

4.3.1 Average and anomaly of temperature indices

Figure 3 illustrates the spatial distribution of the decadal average of TXx computed from the three gridded datasets. The area mean of the decadal average of TXx from CFSR dataset is the greatest (44.7 °C) in comparison to POWER (43.6 °C) and ERA5 (42.3 °C). The TXx values from the three gridded datasets varied between 35 and 48 °C throughout the four decades (1981–2020). The lowest values of TXx are found in the northern coastal zone, southern Sinai, and southwestern Egypt due to the influence of the Mediterranean Sea, Mount Saint Catherine, and Mount Uweinat respectively.

The influence of the Mediterranean climate extends southward to about 26° N (lowest TXx), which agrees with Aboelkhair et al. 2019. The region south of 26° N has the highest values of TXx which gradually increases from 40 to 48 °C over southeast Egypt. The values of TXx vary throughout the four decades, progressively increasing from the first (− 2: + 0.25 °C) to the fourth (− 0.25: + 2 °C) decade as shown by the decadal anomaly in Fig. 3. The decadal

Table 2 The differences (°C) between the observed and estimated highest Tmax values

Date	Day	Aswan			Asyut			Cairo			Arish			Matruh		
		CFSR	ERA5	POWER	CFSR	ERA5	POWER	CFSR	ERA5	POWER	CFSR	ERA5	POWER	CFSR	ERA5	POWER
Jun 1988	28	−1.04	−1.07	0.01	0.81	0.38	1.07	1.94	−1.51	2.72	3.04	−0.12	0.39	−3.22	−2.04	−2.45
	29	−0.21	−0.08	0.48	1.33	−0.38	0.84	1.90	−0.60	3.22	0.36	−2.34	−3.70	−3.32	−2.63	−2.26
	30	−0.61	−0.29	0.27	0.71	−0.76	0.25	3.11	1.06	2.74	−0.09	−2.69	−2.76	−0.25	0.92	0.91
Jun 1995	27	−0.53	−2.82	−0.24	−0.91	−1.82	−0.35	1.70	−0.56	3.49	2.22	−0.88	0.07	−0.66	1.23	0.02
	28	−0.85	−1.69	0.38	−0.74	−1.41	−0.98	2.23	−1.48	2.27	−2.71	−2.13	−3.06	−2.57	−1.61	−2.33
	29	−1.04	−0.81	0.04	0.43	0.50	0.91	3.05	1.50	2.61	2.45	1.05	0.41	1.06	1.07	1.06
	30	−1.40	−0.49	−0.22	−0.98	−0.99	0.04	**3.95**	1.07	2.74	2.65	0.34	0.04	−2.48	−1.94	−0.24
July 2000	27	1.43	−1.13	1.27	2.36	0.27	2.87	3.78	0.19	2.67	3.47	−0.16	0.09	−0.09	0.43	−0.09
	28	1.32	−1.97	−0.31	1.09	−1.76	1.38	2.70	−1.38	3.01	0.85	−2.64	−2.34	1.32	0.20	1.85
	29	0.28	−0.40	0.47	1.25	−0.98	1.77	3.56	−1.51	2.83	1.51	−2.14	−1.81	1.01	1.45	1.85
	30	−0.30	−0.60	−0.06	1.79	−0.18	1.73	1.88	−2.13	1.52	0.47	−1.31	−2.08	1.50	0.14	1.01
	31	−0.24	−0.96	−0.43	1.55	−0.25	1.21	2.35	1.01	2.63	1.31	−2.29	−1.49	0.71	0.78	1.49
July 2002	28	−1.37	−1.23	−0.86	−0.73	−1.67	−0.53	−0.06	−2.78	0.85	0.01	−2.32	−2.84	−3.28	−2.29	−2.78
	29	−1.83	−1.53	−0.38	0.07	−0.83	0.42	0.23	−2.31	0.95	−0.99	−2.62	−2.99	−2.92	−1.41	−2.47
	30	−0.30	−2.82	−0.57	−0.62	−1.94	−0.17	0.79	−2.02	2.11	−0.15	−2.76	−1.78	−2.12	−2.02	−2.06
July 2007	24	−0.69	−1.44	−0.45	0.06	−1.67	0.23	2.63	−0.05	3.12	1.85	−1.52	−1.79	−1.21	−0.27	0.34
	25	−0.64	−2.31	−0.93	−0.32	−1.42	0.00	3.27	−0.26	3.48	1.86	−1.91	−0.84	0.30	1.01	1.76
	26	0.97	−2.77	−1.13	1.79	−2.14	−0.35	1.00	−2.02	1.85	1.91	−1.60	−1.35	−0.46	0.94	1.04
	27	−0.57	−1.86	−0.47	−0.39	−1.46	−0.13	1.14	−1.19	2.03	0.58	−2.48	−1.90	0.75	1.72	1.94
Jun 2010	18	−0.59	−2.49	−1.42	0.15	−1.03	0.30	0.37	−1.32	1.30	0.75	−1.96	−2.70	−2.61	−1.04	−1.62
	19	−1.63	−1.96	−1.26	−1.74	−2.97	−0.76	2.02	0.46	3.07	3.06	−0.58	−0.41	−1.21	−0.02	−0.36
	20	−2.65	−2.44	−2.04	−1.80	−2.49	−2.34	−0.02	−1.67	**−0.01**	−0.99	−2.55	−3.87	−2.03	−0.70	−1.44
	21	0.12	−0.50	0.33	1.64	−0.09	1.46	2.17	−1.33	1.73	3.20	0.20	0.12	−2.44	−2.12	−2.62
August 2015	6	−0.60	−2.37	−1.80	−1.11	−1.75	−0.25	1.74	0.39	3.12	−1.64	−3.74	−3.61	−1.81	−1.58	−0.75
	7	−1.13	−1.87	−0.47	−1.04	−2.51	−1.12	0.46	−0.45	1.60	−2.76	−2.55	−2.93	−0.35	−0.32	−0.03
	8	−1.68	−0.98	−0.23	−0.55	−1.30	−0.18	1.82	0.17	2.45	−2.01	−3.29	−2.54	−0.19	0.08	0.65
	9	−0.97	−0.90	0.21	0.87	0.09	1.84	1.89	0.13	2.83	−2.47	−2.58	−2.55	−1.72	−2.58	−1.18
Jun 2016	20	−1.46	−1.85	−0.76	−0.75	−2.54	−1.05	2.37	0.41	3.15	0.84	−1.27	−0.67	−1.44	−0.57	−0.14
	21	−1.69	−2.25	−1.84	−0.97	−2.24	−1.22	1.52	0.15	2.56	0.58	−0.84	−0.96	0.12	1.63	0.41
	22	−1.92	−2.53	−2.39	0.57	−0.21	0.44	1.90	0.29	2.83	0.59	−1.08	−1.36	1.19	1.61	1.15
	23	−1.39	−2.46	−1.65	0.89	−0.08	1.31	1.87	0.62	2.98	0.50	−1.55	−0.83	0.60	0.96	0.62
Jun 2018	20	−0.22	−0.49	0.84	1.11	0.75	1.02	0.09	−0.38	1.24	−2.01	−3.35	−2.88	−0.55	−0.54	0.73
	21	0.01	**0.09**	1.20	1.82	0.54	1.39	1.51	0.64	1.98	−1.69	−3.07	−3.07	−2.92	−2.72	−2.40
	22	−0.93	−0.66	0.39	−2.38	−2.81	−2.30	0.99	−0.29	1.67	−1.65	−3.70	**−3.91**	0.44	−0.30	1.13
	23	−1.48	−1.28	−1.05	1.56	0.13	0.71	1.53	0.62	2.80	0.66	−0.89	−0.02	0.30	0.42	0.20
Average		−0.74	−1.46	−0.43	0.20	−1.06	0.27	1.81	−0.47	2.35	0.44	−1.81	−1.77	−0.87	−0.35	−0.20

Bold numbers indicate the magnitude of the most significant difference between the observed and estimated highest Tmax values

anomaly of TXx during the first decade over most of Egypt is negative (< 0 °C), which means that the first decade contains TXx values less than the climatological values. The decadal anomaly of TXx increases (− 0.5: + 1 °C) in the second decade and reaches about + 1.5 °C in the third decade. The largest decadal anomaly of TXx (> + 2 °C) is detected during the fourth, especially over the Nile Delta in north.

Figure 4 illustrates the decadal average and decadal anomaly of TXn values during the study period (1981–2020), demonstrating that the TXn values from the three gridded datasets ranged from 5 to 20 °C. The area mean of the decadal average of TXn over Egypt is 14.2 °C, 13.7 °C, and 13.4 °C from POWER, CFSR, and ERA5 respectively. TXn values are below 10 °C in Sinai, the Mediterranean coast and southwestern Egypt, while it exceeds 20 °C in southeastern Egypt. The TXn values along the Red Sea coast exceed 15 °C due to the influence of the Red Sea Mountain ranges. The TXn values are lowest in the second decade compared to the other three decades.

From the climatic point of view, TXn values are low over the Western Desert during the first decade and over the Eastern Desert and Sinai during the second decade, while the last two decades have high TXn values as indicated by the decadal anomaly in Fig. 4. The TXn in eastern Egypt in the first decade is greater than in the second decade by about 2 °C, where its decadal anomalies are about + 1 °C and − 1 °C in the first and second decades, respectively. The third decade has the greatest TXn values compared to the other three decades with positive anomaly (+ 0.5 to + 1.5 °C) except for some negative anomaly (− 0.25 °C) in northern Egypt.

Figure 5 shows the decadal average and decadal anomaly of TNx, where the decadal average ranges between 20 and 30 °C. The decadal average of TNx increased steadily from the first decade to the last decade. The decadal anomaly of TNx indicates that the first decade has the highest negative anomaly values, reaching − 2 in both ERA5 and POWER. At the same time, the CFSR data showed anomaly of up to + 0.5 °C in small and sparse locations. During the second decade, the decadal anomaly of TNx gradually increased and reached more than + 1.5 °C in CFSR and + 0.75 in both POWER and ERA5. The TNx values continue to increase during the third decade as the positive anomalies (+ 0.5) cover larger areas than in the previous two decades. The highest anomalies (> + 1.5 °C) during the fourth decade from the three gridded datasets except the Eastern Desert and South Sinai (− 2 °C) from the CFSR dataset. Overall, a comparison between the first and fourth decades revealed an increase of about 2 °C in TNx values in most of Egypt during the study period.

The geographical distribution of the decadal average and its associated anomaly shown in Fig. 6 reveals that CFSR produces the lowest TNn values (− 5 °C) particularly along the Nile River compared to both EAR5 and POWER. Moreover, the highest values of TNn are found on the coasts of the Mediterranean and the Red Sea, exceeding 5 °C in the three gridded datasets. The ERA5 showed the largest values of TNn along the river (2 – 5 °C) compared to POWER (1 – 4 °C) and CFSR (below − 1 °C). The POWER has the highest area mean value of TNn (2.5 °C) followed by ERA5 (2 °C) and CFSR (0.8 °C).

In addition, the study area covered by the negative (positive) values of TNn gradually decreases (increases) from the first to the fourth decade according to the three gridded datasets, indicating that TNn increased throughout the study period. The decadal anomaly of TNn in northern and eastern Egypt did not exceed + 0.5 °C during the first decade with prevailing values ranging from + 0.5 to − 0.5 °C. While the decadal anomaly of TNn increased to more than + 1 °C in ERA5 and + 0.5 °C in both CFSR and POWER during the second decade. The positive decadal anomaly of TNn exceeds + 1 °C in the third decade especially in the ERA5 data with some negative anomaly values in both CFSR and ERA5. The decadal anomalies increased by + 2 °C in the fourth decade compared to the first decade in central and southern Egypt, although ERA5 and CFSR had the lowest anomalies in northwestern and eastern Egypt respectively. Thus, the decadal anomaly of TNn did not exceed + 0.5 °C in the first decade but increased gradually throughout the decades up to more than + 2 °C in the fourth decade.

4.3.2 Trend and COV of temperature indices

Figure 7 shows the Mann–Kendall rank correlation (Tau) and the coefficient of variation (COV) to illustrate and characterize the TXx trend and variability throughout Egypt. A positive Tau trend dominates in the first decade, with values ranging from − 0.3 to + 0.3 except southern Sinai, Eastern Desert, and southern Egypt that have Tau higher than + 0.3 and exceed + 0.9 in Aswan. The second and third decades are dominated by negative Tau values higher than − 0.6, indicating a significant negative trend, particularly in the Western Desert and the majority of the Nile Valley. Tau has positive values (+ 0.3 to + 0.6) in the second decade in the Nile Delta, southern Sinai, Red Sea coastal region, southwest Egypt, and the Eastern Desert. In the fourth decade, Tau ranges from − 0.3 to + 1 over most of Egypt with higher positive (most significant) Tau in Western Desert, northern Sinai, and northwest Egypt. From the first to the third decade, low COV values (< 2) spread across southern and southwestern Egypt and south Sinai in the fourth decade. While COV values more than 2 up to 5 are common in other areas, particularly in the northern coastal range. The COV values indicate that TXx variability increased in the second decade compared to the first decade, particularly in ERA5, while POWER showed the lowest variability. The geographical distribution of COV values is negatively

Table 3 The differences (°C) between the observed and estimated lowest Tmin values

Date	Day	Aswan			Asyut			Cairo			Arish			Matruh		
		CFSR	ERA5	POWER	CFSR	ERA5	POWER	CFSR	ERA5	POWER	CFSR	ERA5	POWER	CFSR	ERA5	POWER
Jan 1987	10	−2.44	−1.61	−3.32	−3.37	2.04	2.45	−2.69	−2.33	−3.47	−0.22	−0.87	−0.92	2.90	−0.07	0.80
	11	−2.06	−0.26	−3.05	−1.46	2.27	2.62	−2.35	1.20	−2.57	−0.77	−1.58	0.67	2.57	1.44	2.51
	12	−2.71	−0.26	−2.43	−2.53	1.90	2.26	−3.47	−2.43	−2.94	3.07	0.26	3.28	3.50	2.78	2.15
Jan 1989	5	−3.01	1.87	−0.39	1.70	0.98	−1.87	**0.87**	−0.49	−2.28	2.27	1.78	1.54	0.15	−1.49	−0.13
	6	1.95	1.34	3.74	−1.21	0.33	−2.00	−3.43	−2.11	−3.03	0.97	1.36	3.83	−0.36	0.95	0.37
	7	−3.68	−0.74	−2.21	−2.24	−1.24	−0.89	−2.40	−1.09	−1.83	2.13	1.76	2.26	3.40	2.05	2.37
	8	−2.93	−0.69	−3.35	−0.99	2.11	−2.04	−3.47	−1.81	−2.63	3.23	1.56	2.06	2.95	2.84	2.25
Feb 1992	8	−2.08	−1.01	−2.95	−1.72	2.41	−0.99	−1.61	−0.99	−1.35	−0.25	−1.14	0.05	2.53	2.11	3.25
	9	−2.01	−0.48	−2.80	−3.16	1.24	−2.44	0.27	−2.19	−2.28	1.96	0.65	2.00	0.26	0.17	**−0.20**
	10	3.37	1.38	3.20	−1.45	−0.04	−0.08	−2.28	−2.28	−2.78	1.25	1.40	2.86	1.33	0.78	1.04
	11	−2.38	−1.56	−3.21	−2.35	1.21	−0.83	−1.45	−2.00	−2.36	1.34	0.68	1.36	3.83	2.50	3.65
Jan 1993	12	**−3.93**	0.00	−2.30	−2.17	2.24	−1.86	−0.74	−0.09	−2.13	2.67	0.99	3.01	3.27	1.55	2.80
	13	−2.34	0.20	−1.72	−3.08	0.98	−1.01	−2.20	−1.42	−1.11	2.75	1.39	2.20	3.03	1.41	3.71
	14	−2.09	−0.05	−0.76	−2.25	1.13	−0.12	−1.74	−0.38	−0.75	2.84	1.48	2.31	2.88	1.54	3.83
Jan 2000	28	−2.15	0.51	−2.10	0.82	1.61	−0.69	−1.68	−1.86	−1.90	2.25	1.95	3.34	1.01	1.20	1.08
	29	−3.86	−0.74	−2.21	1.21	−0.24	−2.07	0.64	−1.46	−3.20	1.96	0.98	1.78	3.96	2.38	2.64
	30	−3.82	0.54	−1.94	−3.11	2.79	0.42	−3.04	−0.32	−0.75	3.23	0.99	2.85	2.38	1.02	1.61
	31	−3.37	0.03	−2.51	−0.45	1.19	−0.27	−3.81	0.17	−0.92	3.33	3.65	3.59	2.03	0.37	0.42
Feb 2003	25	−2.46	−0.02	−1.68	−2.89	−0.50	−1.19	−1.08	−2.04	−2.82	−0.15	−0.44	0.35	3.74	1.80	2.93
	26	−3.80	0.06	−1.89	−2.59	0.18	−0.57	−0.49	−1.66	−3.27	1.10	1.23	1.94	2.44	1.18	1.86
	27	−3.46	−0.04	−1.99	−2.36	−0.48	−1.10	−2.20	−2.17	−3.67	−0.32	0.47	1.37	2.11	−0.07	2.02
Jan 2005	18	−2.29	−1.47	−1.21	−2.37	−0.33	−2.57	−1.95	−1.85	−3.10	2.89	1.55	2.79	3.41	0.90	2.99
	19	−2.73	−0.84	−1.45	−1.52	0.85	−0.74	0.76	−1.16	−1.61	2.49	2.26	2.70	2.43	2.11	3.01
	20	−2.56	−0.87	−1.70	−3.00	−0.44	−0.01	−3.07	−2.96	−2.35	0.99	0.07	1.20	2.38	0.60	1.73
	21	−2.30	−0.10	−1.96	0.34	0.72	1.06	−2.11	−2.72	−3.80	2.77	0.00	2.44	3.68	1.75	1.39
Jan 2008	13	−2.97	0.92	−1.64	−1.80	2.03	−0.46	−0.79	−0.55	−1.50	3.79	2.19	2.70	2.02	0.30	1.61
	14	−2.47	0.04	−2.61	0.00	2.99	0.76	−0.68	0.38	−1.47	2.65	1.41	3.93	1.98	0.87	1.83
	15	−2.44	0.34	−2.30	−1.62	2.03	−0.55	−1.91	−1.05	−2.16	3.16	3.27	2.76	2.26	1.26	3.10
	16	−2.51	0.58	−1.91	−2.30	2.33	2.73	−2.31	−0.46	−2.98	2.59	3.68	2.86	2.07	1.15	2.53
	17	−3.53	1.95	−0.81	−2.69	2.33	2.81	−1.14	−0.60	−2.47	**3.98**	0.81	3.97	2.92	2.00	2.68
Jan 2009	3	−3.72	0.73	−1.39	−2.76	2.79	1.87	−3.43	−2.09	−3.78	2.78	0.87	2.27	3.53	2.06	3.76
	4	−3.64	0.47	−2.38	−2.02	1.11	1.25	−3.17	−2.28	−1.99	1.97	0.23	2.23	3.05	2.81	2.78
	5	−2.75	−0.65	−2.98	−2.66	2.24	2.61	−2.93	−2.23	−1.31	3.19	0.20	3.44	3.91	1.93	2.63

Table 3 (continued)

Date	Day	Aswan			Asyut			Cairo			Arish			Matruh		
		CFSR	ERA5	POWER	CFSR	ERA5	POWER	CFSR	ERA5	POWER	CFSR	ERA5	POWER	CFSR	ERA5	POWER
Jan 2012	10	−2.46	−1.42	−2.53	−2.74	1.86	2.49	−3.18	−2.15	−3.86	2.36	0.85	2.62	1.12	0.65	0.11
	11	−1.99	−0.37	−1.58	−1.65	0.71	−2.00	−2.38	−1.16	−2.42	2.80	2.15	2.91	2.14	0.52	1.84
	12	−3.05	0.07	−2.57	−2.39	0.40	−1.06	−2.43	−1.83	−2.24	2.23	1.71	1.97	2.41	0.57	2.47
	13	−2.55	−0.43	−3.21	−1.85	1.50	−1.70	−0.45	−0.90	−2.36	0.63	0.63	0.52	2.97	1.59	2.92
Jan 2016	28	−2.30	0.65	−1.62	−1.31	1.67	−0.34	−0.94	−1.46	−2.22	2.33	3.15	2.23	2.59	1.29	2.62
	29	−2.80	−1.43	−3.65	0.56	1.73	−1.16	−2.58	−0.66	−2.04	3.67	1.84	3.67	3.10	2.01	3.05
	30	−2.50	−0.61	−2.64	−0.39	1.37	−0.59	−2.48	−2.64	−3.60	2.75	−0.07	2.70	3.02	1.00	3.66
	31	−3.73	−0.28	−1.97	1.80	2.52	0.54	−2.33	−1.23	−2.28	2.33	2.07	2.93	3.42	1.47	2.13
Jan 2017	3	−3.24	−0.54	−1.58	−1.69	1.22	−1.17	−3.75	−2.28	−3.35	2.16	3.10	3.27	3.20	1.69	3.28
	4	−3.67	1.41	−0.73	−0.40	1.12	−1.22	−3.24	−2.99	−2.10	2.87	2.05	3.40	1.39	−0.62	1.42
	5	−3.31	−0.40	−1.60	−2.75	−0.60	−0.84	−3.65	−2.16	−2.93	2.22	1.54	3.72	3.04	1.21	2.90
	6	−3.55	−0.01	0.04	−2.18	2.02	2.26	−2.37	−1.78	−1.46	3.79	2.58	3.86	2.29	1.49	3.49
Average		−2.63	−0.08	−1.82	−1.62	1.25	−0.18	−2.02	−1.48	−2.39	2.18	1.26	2.42	2.54	1.27	2.24

Bold numbers indicate the magnitude of the most significant difference between the observed and estimated lowest Tmin values

correlated with Tau values, where their correlation ranges between −0.3 and −0.5 during the first two decades, while it ranges from −0.1 to −0.25 during the last two decades in the three gridded datasets.

Figure 8 shows the values of the spatial distribution of the decadal Tau and COV for TXn, where the first decade indicates a positive Tau throughout the study region except the Western Desert in the CFSR data and some scattered locations in northern Egypt in the ERA5. The three gridded datasets produce positive Tau values higher than +0.3 over the Red Sea coast and southeast Egypt.

The second decade is marked by a general positive Tau (>0) except over southern Nile Valley in CFSR. The three gridded datasets almost have the highest positive Tau values (>+0.3) throughout the third decade. It is noticed that the negative Tau values increased in the fourth decade, especially in the Western Desert, to reach less than −0.3 near the Libyan borders, where ERA5 has the greatest Tau values and POWER has the lowest Tau. Moreover, the lowest COV values (<10) covered large area in the first and fourth decades, and the highest COV values (>10) covered the large area in the second and third decades, where the highest variability (COV>20) appears in the eastern delta, Sinai, and sometimes in southwestern Egypt. Sometimes sites with high COV values correspond to places with low Tau values of TXn where the correlation is negative (−0.04 to −0.13) during the first decade and positive (0.04 to 0.5) during the other three decades.

The spatial distribution of decadal Tau and COV for TNx is shown in Fig. 9, where the Tau values ranging from −0.6 to +0.9 during the selected four decades. Furthermore, the significant negative trend (Tau > −0.6) is found in a few regions like in the western borders from CFSR and Eastern Desert from POWER. Also, the CFSR exhibit positive Tau values (>+0.3) and increases to +0.9 in specific areas (middle of the Western Desert and southeast Egypt), and it rarely exceeds +0.6 in both EAR5 and POWER datasets. During the second decade, the areas covered by the negative Tau values (<−0.3) increased over separate locations in the Western Desert, while the positive Tau (+0.3 to +0.6) still dominates most of Egypt in POWER and ERA5. The negative Tau (<0) values of TNx in the third decade covered the largest area, while the significant positive Tau (>+0.3) dominated most of Egypt in the fourth decade with small scattered negative Tau values (>−0.3). The CFSR is producing higher COV values for TNx Than both ERA5 and POWER during the study period. Furthermore, the spatial distribution of the decadal COV of TNx is negatively correlated with its corresponding decadal Tau of TNx during the first three decades which ranges from −0.01 to −0.5, while the fourth decade has a positive correlation (0.04 to 0.2).

For the TNn, the geographical distribution of the decadal Tau and COV are shown in Fig. 10. The highest negative

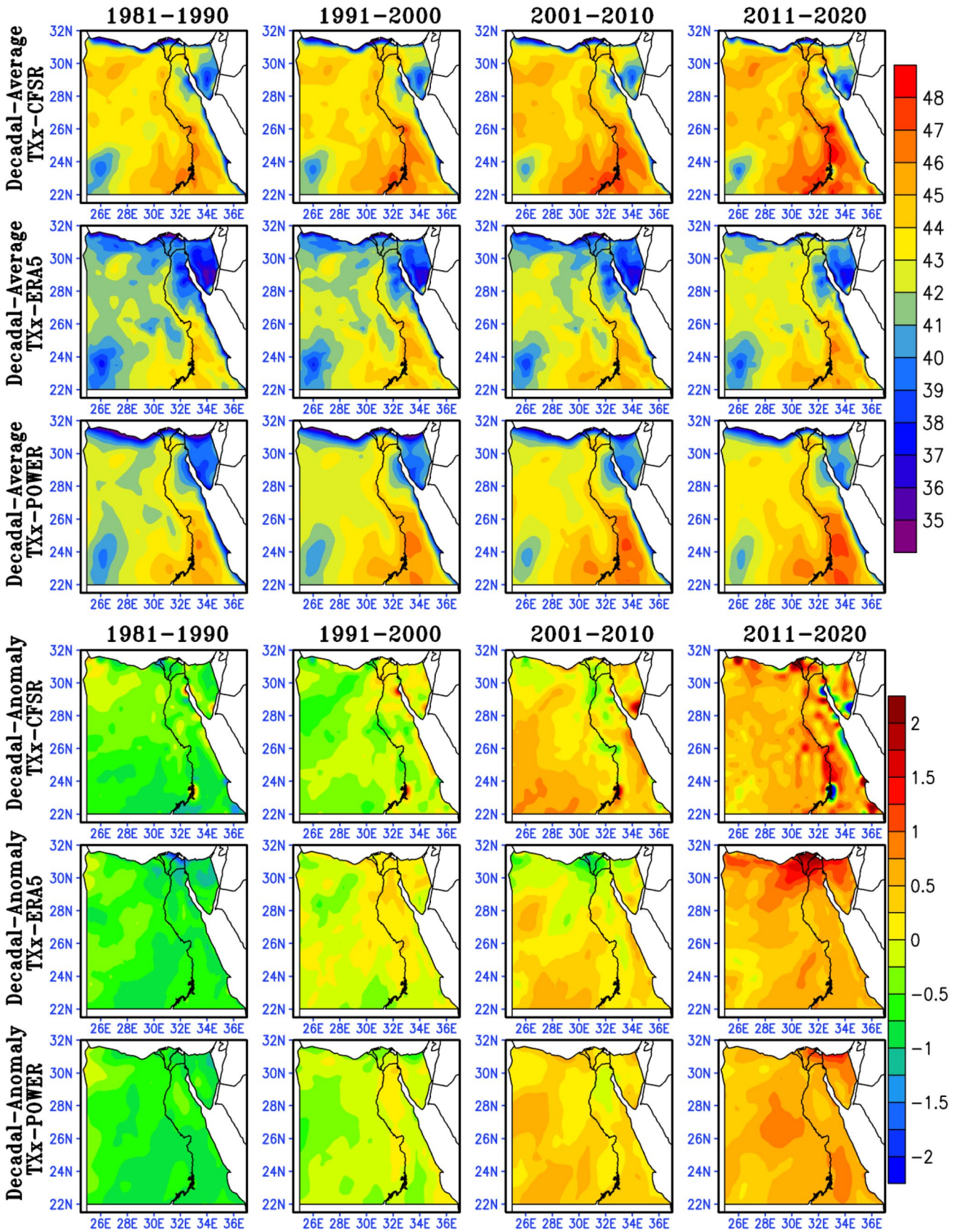

Fig. 3 Spatial distribution of the decadal average and decadal anomaly of TXx

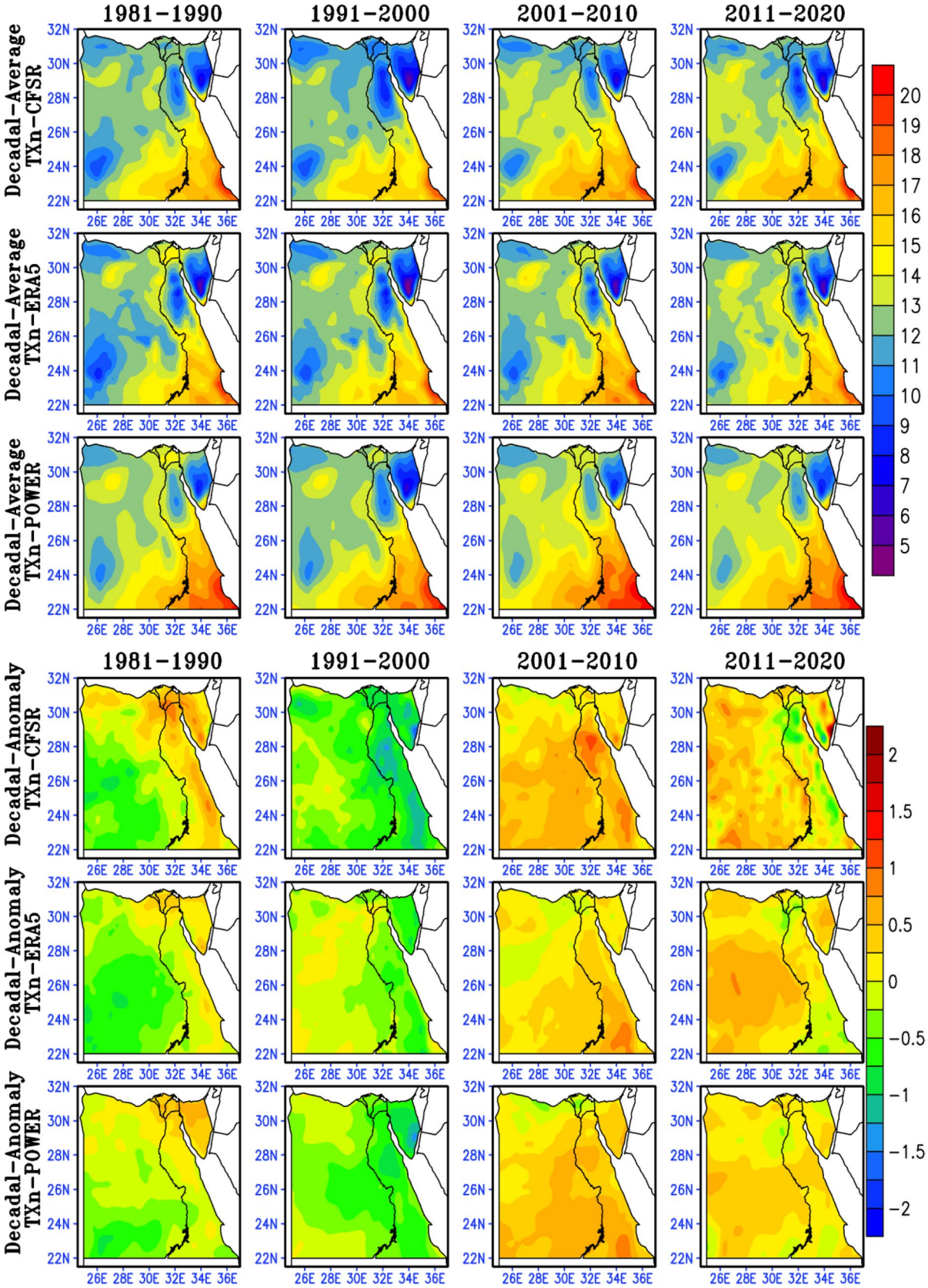

Fig. 4 Spatial distribution of the decadal average and decadal anomaly of TXn

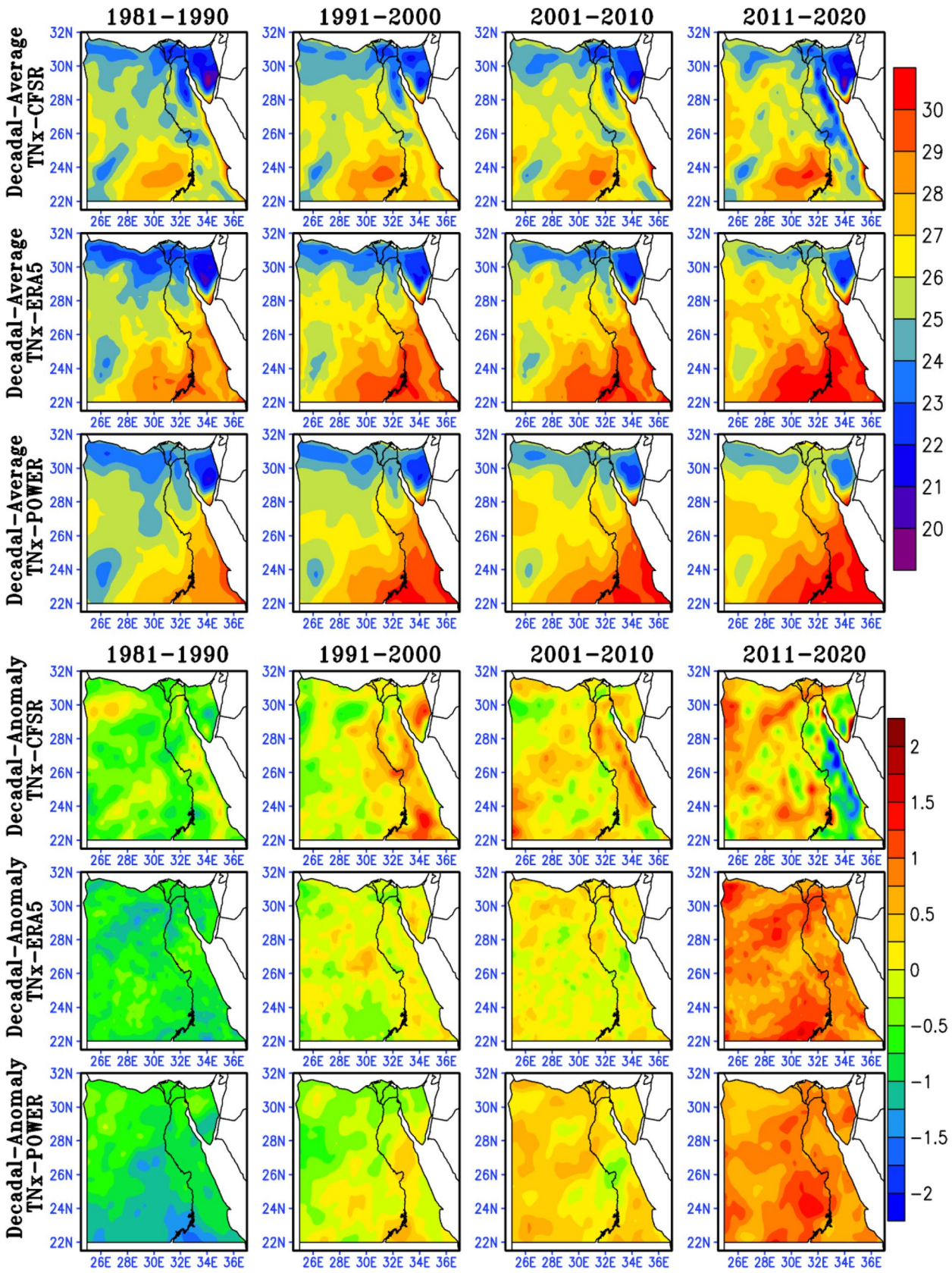

Fig. 5 Spatial distribution of the decadal average and decadal anomaly of TNx

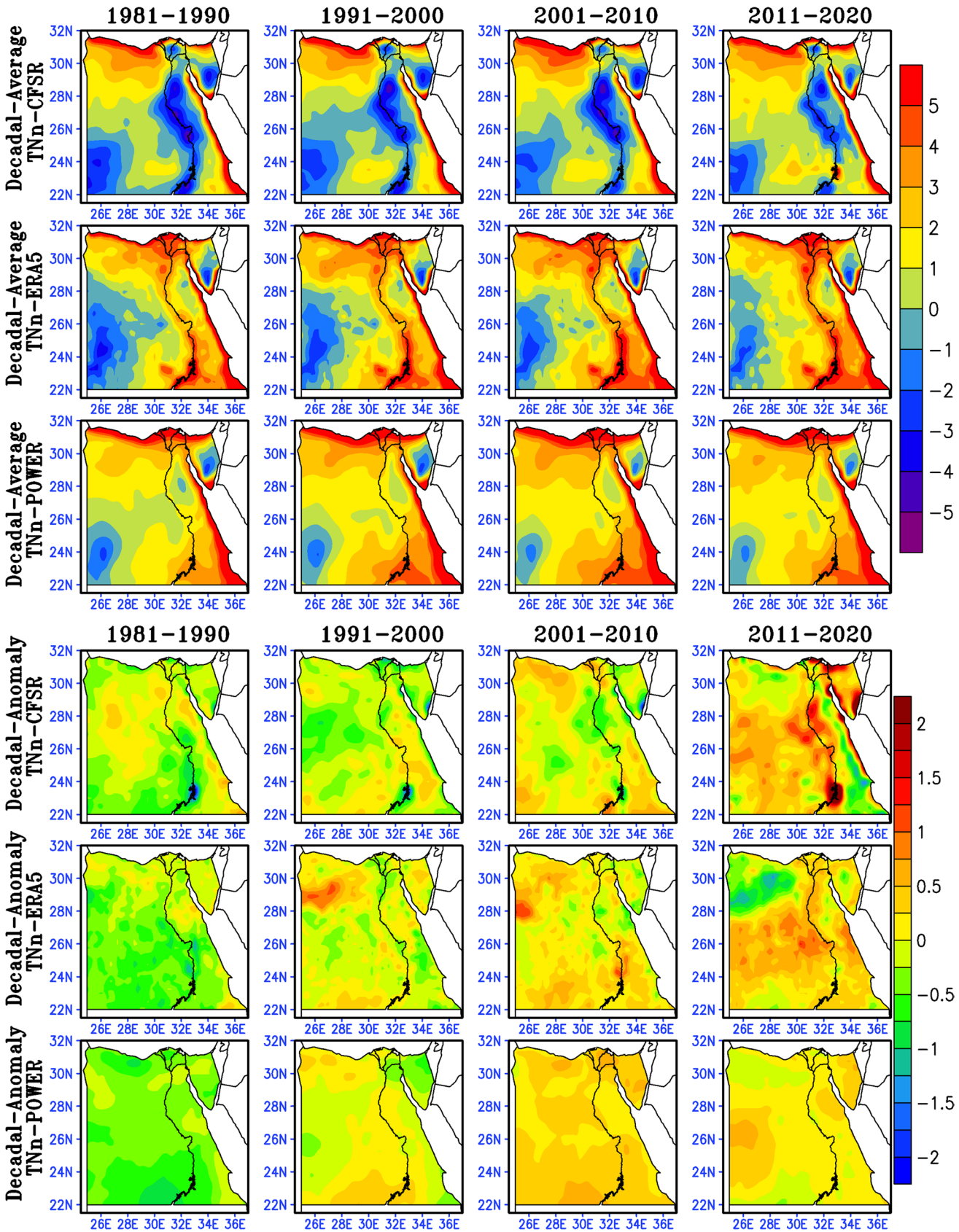

Fig. 6 Spatial distribution of the decadal average and decadal anomaly of TNn

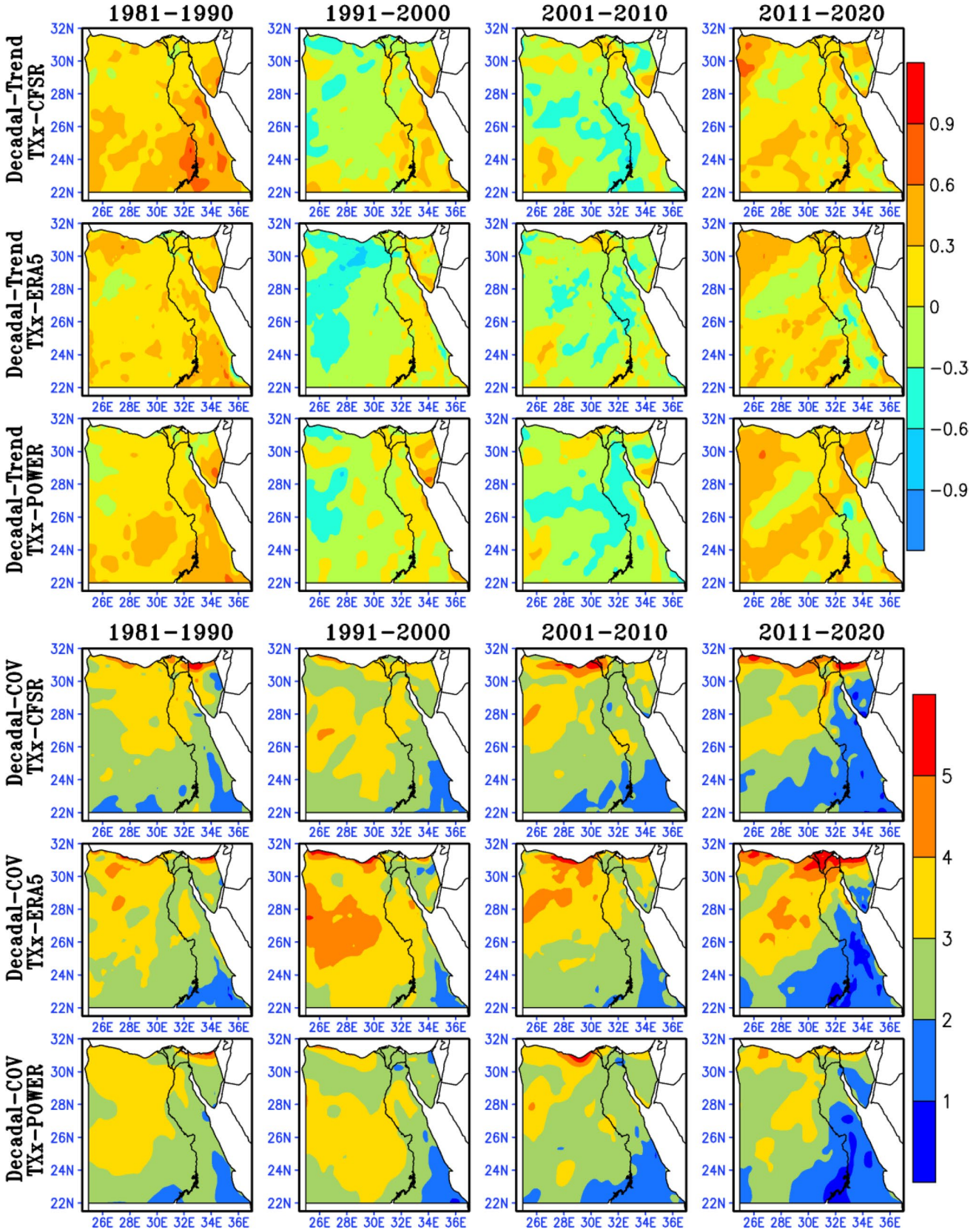

Fig. 7 Geographical distribution of the decadal Mann–Kendall rank correlation (Tau) and decadal coefficient of variation (COV) for TXx

Tau values of TNn (> −0.6) in the first decade is detected in CFSR at different locations in Sinai and Eastern Desert. While the positive Tau values (> +0.3) are mainly found in the Western Desert and northern part of the Eastern Desert. The positive Tau values for TNn dominate in EAR5 followed by POWER, where the highest positive Tau values (significant trend) ranges from +0.3 to +0.9 are detected in northern Egypt and dispersed regions along the Red Sea coast. In the second decade, the negative Tau values of TNn appears in a small area in north of Egypt and gradually increase to record the highest positive Tau of TNn (+0.9) in southern Egypt in the CFSR.

In the third decade, the most negative Tau values of TNn (−0.3 to −0.6) are found in Sinai, while the significant trend (Tau > +0.6) appears in the Eastern Desert in EAR5 and POWER and in the Western Desert in CFSR. In the fourth decade, most of Egypt has negative Tau values of TNn which never occurred in any of the first three decades, where the positive Tau values of TNn are only found in Sinai, southeast Egypt, and sometimes northern Egypt as in POWER. The decadal COV values of TNn less than 5 dominate over the Mediterranean and Red Sea coasts, while COV values of 6–12 dominate over Western Desert and Sinai in the three gridded datasets during all decades.

Additionally, it is detected that the variability of TNn is higher in CFSR than in both POWER and ERA5. Finally, the correlation between the spatial distribution of decadal COV and Tau of TNn overall decades is mostly negative and ranges from −0.6 to +0.3. The findings for the selected indices (TXx, TXn, TNx, and TNn) are in great agreement with the results of several studies of extreme warm and cold events worldwide (e.g., Sun et al. 2016; Wang et al. 2017).

5 Conclusions

Daily data for maximum (Tmax) and minimum (Tmin) temperatures were downloaded from three gridded reanalysis datasets (ERA5, CFSR, and POWER) for four consecutive decades (1981–2020) to study the variability of extreme warm and cold events over Egypt. The Tmax and Tmin of the three reanalysis datasets were evaluated against the observations at 24 in-site stations and showed a good agreement and can be employed appropriately to interpret extreme warm and cold temperature events in Egypt. Furthermore, the monthly maximum value of daily Tmax (TXx), monthly minimum value of daily Tmax (TXn), monthly maximum value of daily Tmin (TNx), and monthly minimum value of daily Tmin (TNn) were calculated using the climate data operator (CDO) tool to investigate the variability of extremes over Egypt.

The main findings of this study can be summarized as follows:

- The area mean of the decadal average of TXx from the CFSR dataset (44.7 °C) is higher than both POWER (43.6 °C) and ERA5 (42.3 °C).
- The decadal anomaly of TXx increased to +1, +1.5, and more than +2 °C in the second, third, and fourth decades respectively.
- The Mann–Kendall rank correlation (Tau) for TXx is mostly positive in the first and fourth decades and mostly negative in the second and third decades.
- The lowest coefficient of variation (COV) for TXx is less than 2 and detected in southern and southwestern Egypt and sometimes in Sinai, and ranges from 1 to 5 over Egypt across all decades.
- The area mean of the decadal average of TXn from POWER (14.2 °C) is greater than both CFSR (13.7 °C) and ERA5 (13.4 °C).
- The third decade has the greatest TXn values with a positive anomaly between +0.5 and +1.5 °C except for northern Egypt (−0.25 °C).
- All decades almost have positive Tau values of TXn, but the third decade has a significant positive trend (Tau > +0.6), and the fourth decade has a significant negative trend (Tau < −0.3).
- The first and fourth decades have the lowest COV values (< 10) for TXn over most Egypt, while the second and third decades have the highest COV values (> 10) over most Egypt.
- The area mean of the decadal average of TNx is the greatest (27.5 °C) in ERA5 as compared to both POWER (27 °C) and CFSR (26 °C).
- The highest negative decadal anomaly of TNx (−2 °C) is detected in first decade and increased gradually up to the highest positive anomaly in the last decade (+2 °C) in most of Egypt.
- Tau values for TNx from the three gridded datasets indicate that the significant positive trends (> +0.3) are detected in the fourth decade followed by the first decade, while the significant negative trends (< −0.3) are found in the third decade followed by the second decade.
- CFSR produces higher COV values for TNx (> 7) than both ERA5 and POWER throughout the selected four decades over Egypt.
- The area mean value of the decadal average of TNn from CFSR (0.8 °C) is lower than both EAR5 (2 °C) and POWER (2.5 °C).
- The decadal anomaly was less than +0.5 °C in the first decade but exceed +2 °C in the fourth decade, indicating that TNn increased gradually throughout the study period (1981–2020).
- The significant positive trend of TNn (Tau > +0.3) appears during the third decade followed by the second decade, while the significant negative trend (Tau < −0.3) occurs during the fourth decade.

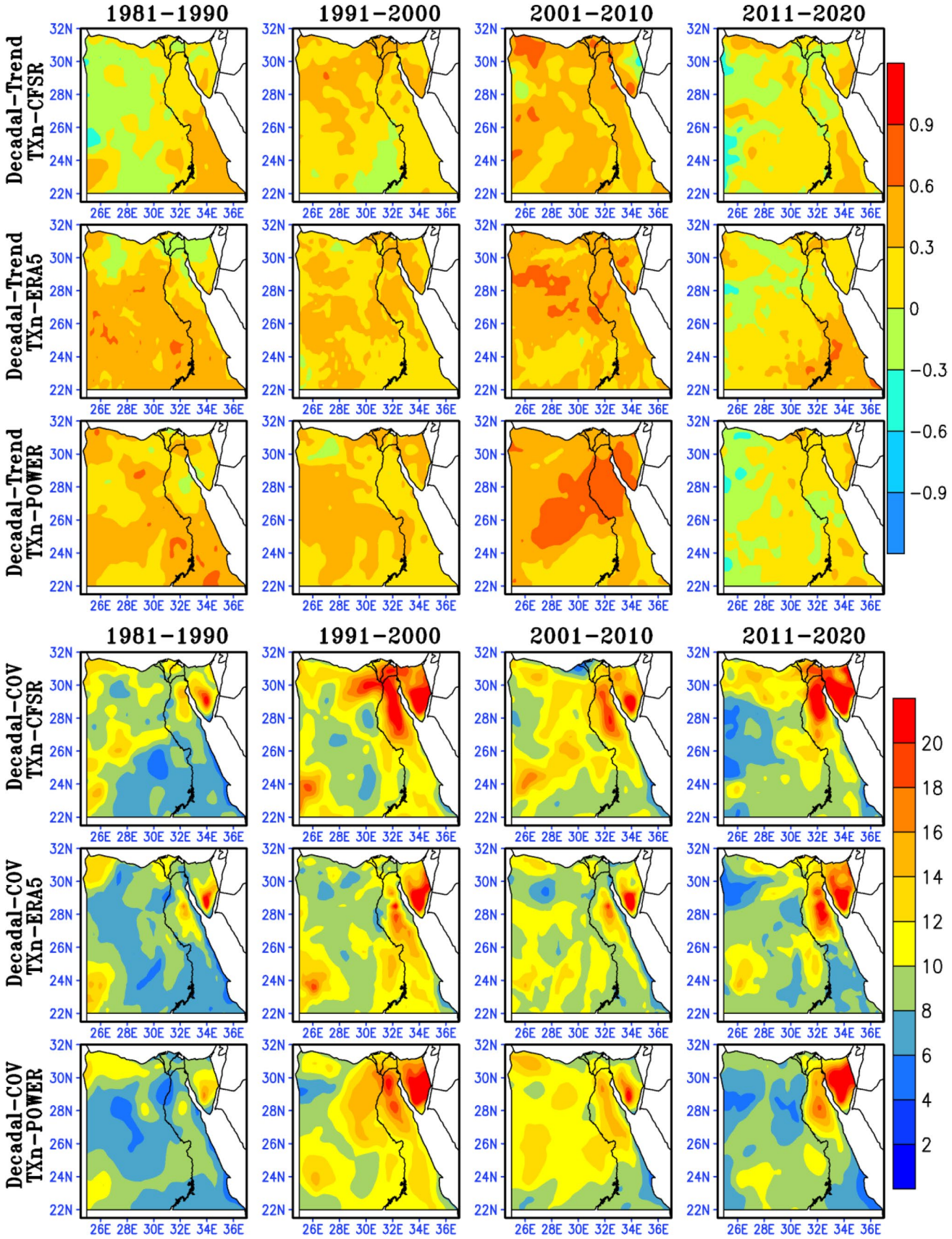

Fig. 8 Geographical distribution of the decadal Mann–Kendall rank correlation (Tau) and decadal coefficient of variation (COV) for TXn

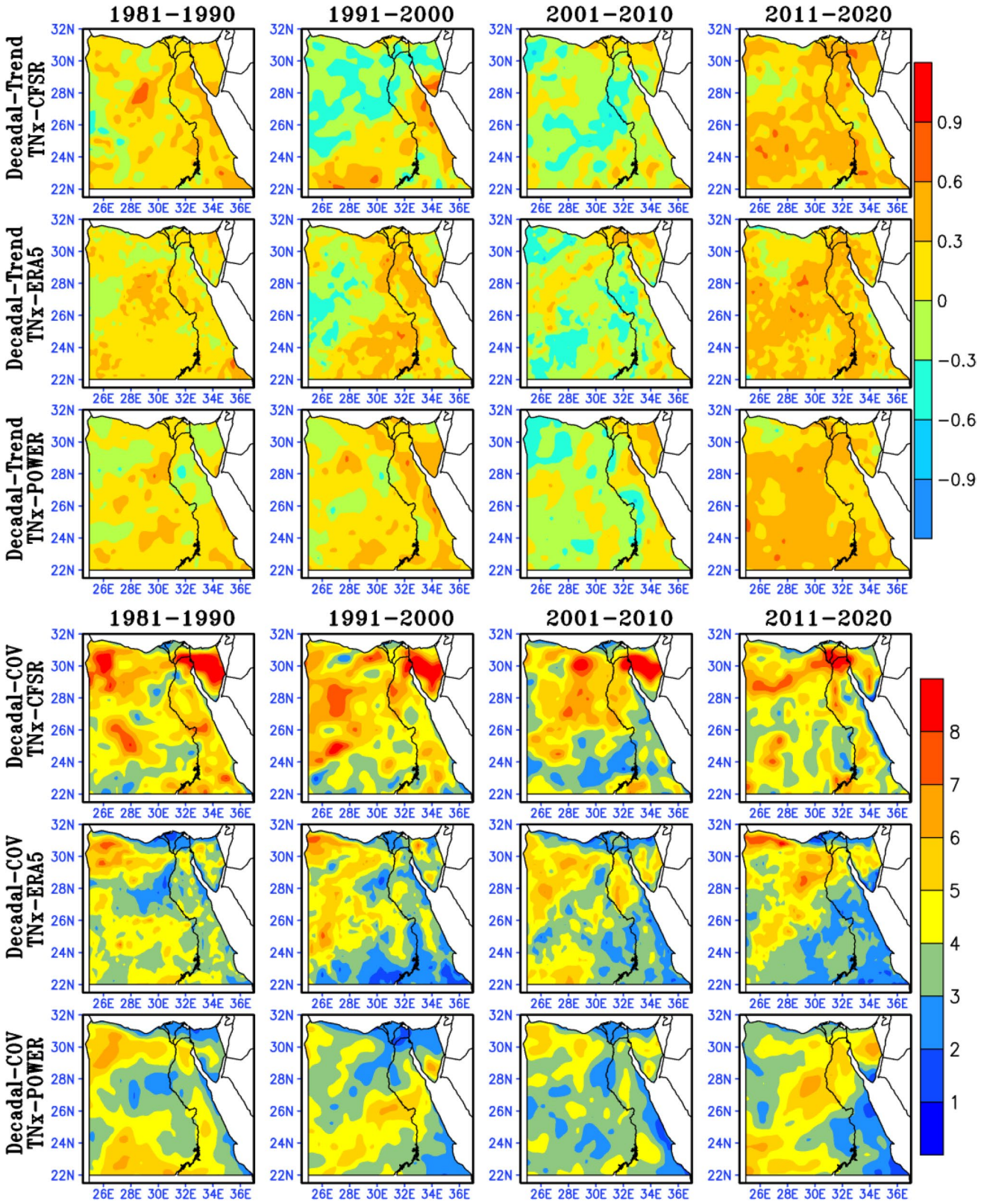

Fig. 9 Geographical distribution of the decadal Mann–Kendall rank correlation (Tau) and decadal coefficient of variation (COV) for TNx

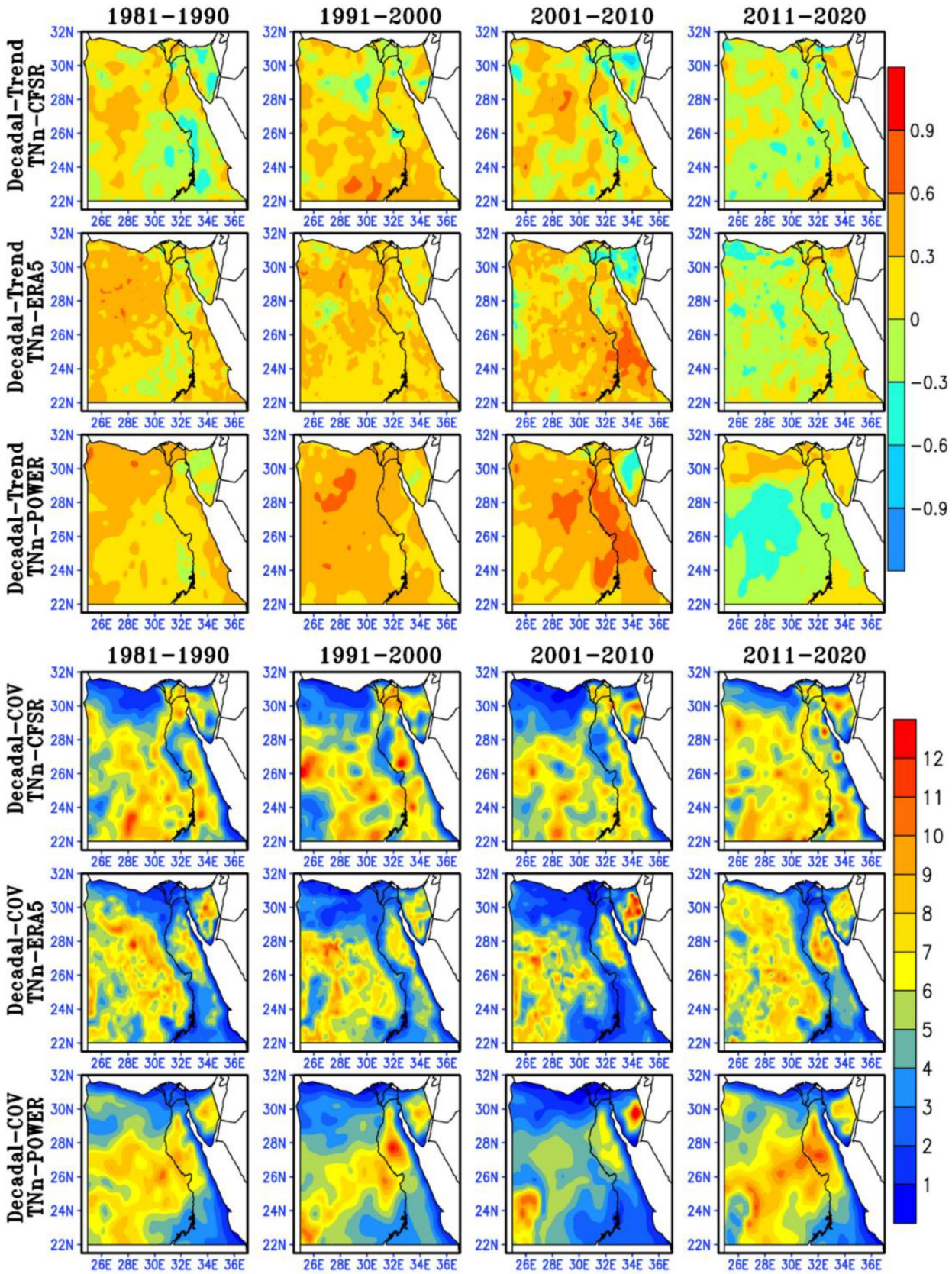

Fig. 10 Geographical distribution of the decadal Mann–Kendall rank correlation (Tau) and decadal coefficient of variation (COV) for TNn

- The lowest decadal COV values of TNn (< 5) are detected over the Mediterranean and Red Sea coasts, while the highest COV values (6–12) dominate most of the Western Desert and Sinai.
- Generally, the COV and Tau of all indices over Egypt are often negatively correlated (> − 0.5).
- Finally, one can conclude that the significant increase in the trend of extreme warm and the slight decrease in the trend of extreme cold are due to the climatic increase in both mean and variance of temperature over Egypt.

Author contribution H.A. and M.M. contributed to the study conception, idea, and design. Methodology, data collection and analysis, visualization, and discussion of results were performed by H.A. and M.M. The first draft of the manuscript was written and prepared by H.A. and M.M. Also, H.A. and M.M. did the writing—review and editing. All authors have read and approved the final version of the manuscript.

Funding Open access funding provided by The Science, Technology & Innovation Funding Authority (STDF) in cooperation with The Egyptian Knowledge Bank (EKB).

Data availability The data used to support the findings of this article were obtained from four freely available sources:

1- GSOD Observed data from NOAA/NCEI website https://www.ncei.noaa.gov/maps/daily/, which accessed on 01-May-2021.

2-NASA/POWER gridded data from the POWER Regional Data Access widget https://power.larc.nasa.gov/data-access-viewer/, which accessed on 01-May-2021.

3-ECMWF/ERA5 gridded reanalysis data from C3S-CDS website https://cds.climate.copernicus.eu/, which accessed on 03-May-2021.

4- NCEP/CFSR gridded reanalysis data from NCAR/RDA website https://rda.ucar.edu/datasets/, which accessed on 05-May-2021.

Code availability The Geographic Information System (ArcGIS 10.8) software, Grid Analysis and Display System (GrADS), R software environment, Climate Data Operator (CDO), and Microsoft Excel are the used programs to accomplish the different methodology, data analysis, and visualization.

Declarations

Ethics approval Not applicable.

Consent to participate Not applicable.

Consent for publication Not applicable.

Competing interests The authors declare no competing interests.

References

Abatan AA, Abiodun BJ, Lawal KA, Gutowski WJ Jr (2016) Trends in extreme temperature over Nigeria from percentile-based threshold indices. Int J Climatol 36(6):2527–2540

Abba SI, Linh NTT, Abdullahi J, Ali SIA, Pham QB, Abdulkadir RA, Costache R, Anh DT (2020) Hybrid machine learning ensemble techniques for modeling dissolved oxygen concentration. IEEE Access 8:157218–157237

Aboelkhair H, Morsy M, El Afandi G (2019) Assessment of agroclimatology NASA POWER reanalysis datasets for temperature types and relative humidity at 2 m against ground observations over Egypt. Adv Space Res 64(1):129–142

Almazroui M, Islam MN, Saeed S, Alkhalaf AK, Dambul R (2017) Assessment of uncertainties in projected temperature and precipitation over the Arabian Peninsula using three categories of CMIP5 multimodel ensembles. Earth Syst Environ 1:23. https://doi.org/10.1007/s41748-017-0027-5

Bai J, Chen X, Dobermann A, Yang H, Cassman K, Zhang F (2010) Evaluation of NASA satellite- and model-derived weather data for simulation of maize yield potential in China. Agron J 102(1):9–16

Chai T, Draxler RR (2014) Root mean square error (RMSE) or mean absolute error (MAE)?–Arguments against avoiding RMSE in the literature. Geosci Mod Dev 7(3):1247–1250

Chikabvumbwa SR, Salehnia N, Manzanas R, Abdelbaki C, Zerga A (2022) Assessing the effect of spatial–temporal droughts on dominant crop yield changes in Central Malawi. Environ Monit Assess 194:63. https://doi.org/10.1007/s10661-021-09709-4

Driouech F, ElRhaz K, Moufouma-Okia W, Arjdal K, Balhane S (2020) Assessing future changes of climate extreme events in the CORDEX-MENA region using regional climate model ALADIN-Climate. Earth Syst Environ 4:477–492. https://doi.org/10.1007/s41748-020-00169-3

Duarte YC, Sentelhas PC (2020) NASA/POWER and Daily Gridded weather datasets-how good they are for estimating maize yields in Brazil? Int J Biometeor 64(3):319–329

El Kenawy AM, Hereher ME, Robaa SM (2019a) An assessment of the accuracy of MODIS land surface temperature over egypt using ground-based measurements. Remote Sens 11(20):2369. https://doi.org/10.3390/rs11202369

El Kenawy AM, Lopez-Moreno JI, McCabe MF, Robaa SM, Domínguez-Castro F, Peña-Gallardo M, Trigo RM, Hereher ME, Al-Awadhi T, Vicente-Serrano SM (2019b) Daily temperature extremes over Egypt: spatial patterns, temporal trends, and driving forces. Atmos Res 226:219–239

Gauch HG, Hwang JTG, Fick GW (2003) Model evaluation by comparison of model-based predictions and measured values. Agron J 95:1442–1446

Gebrechorkos SH, Hülsmann S, Bernhofer C (2019) Changes in temperature and precipitation extremes in Ethiopia, Kenya, and Tanzania. Int J Climatol 39(1):18–30

Gleixner S, Demissie T, Diro GT (2020) Did ERA5 improve temperature and precipitation reanalysis over East Africa? Atmosphere 11(9):996

Hersbach H, Bell B, Berrisford P, Biavati G, Horányi A, Muñoz Sabater J, Nicolas J, Peubey C, Radu R, Rozum I, Schepers D, Simmons A, Soci C, Dee D, Thépaut JN (2018) ERA5 hourly data on single levels from 1979 to present. Copernicus Climate Change Service

(C3S) Climate Data Store (CDS). Accessed on 03-May-2021. https://doi.org/10.24381/cds.adbb2d47
Kendall MG (1970) The measurement of rank correlation. Rank Correlation Methods, 4th ed.; Charles Griffin: London, UK. pp 1–18
Lelieveld J, Hadjinicolaou P, Kostopoulou E, Chenoweth J, El Maayar M, Giannakopoulos C, Hannides C, Lange MA, Tanarhte M, Tyrlis E, Xoplaki E (2012) Climate change and impacts in the Eastern Mediterranean and the Middle East. Clim Change 114:667–687
Lott N, Baldwin R, Jones P (2001) The FCC integrated surface hourly database: a new resource of global climate data
Moriasi DN, Arnold JG, Van Liew MW, Bingner RL, Harmel RD, Veith TL (2007) Model evaluation guidelines for systematic quantification of accuracy in watershed simulations. Amer Soc Agric Biol Eng 50(3):885–900
Morsy M, El Afandi G (2021) Decadal changes of heatwave aspects and heat index over Egypt. Theoret Appl Climatol 146(1):71–90
Nashwan MS, Shahid S, Abd Rahim N (2019) Unidirectional trends in annual and seasonal climate and extremes in Egypt. Theoret Appl Climatol 136(1):457–473
Ouda S, Morsy M, Sayad T, El Hussieny F (2015) Parameterization of CropSyst model for four wheat cultivars grown in Egypt. Global J Adv Res 2(6):851–861
Patakamuri SK, O'Brien N, Patakamuri MSK (2020) Package 'modifiedmk'. Cran. R-project
Peterson TC, Easterling DR, Karl TR, Groisman P, Nicholls N, Plummer N, Torok S, Auer I, Boehm R, Gullett D, Vincent L, Heino R, Tuomenvirta H, Mestre O, Szentimrey T, Salinger J, Førland EJ, Hanssen-Bauer I, Alexandersson H, Jones P, Parker D (1998) Homogeneity adjustments of in situ atmospheric climate data: a review. Int J Climatol 18(13):1493–1517
Pineiro G, Perelman S, Guerschman J, Paruelo J (2008) How to evaluate models: observed vs. predicted or predicted vs observed? Ecol Model 216:316–322
Rodrigues GC, Braga RP (2021) Evaluation of NASA POWER reanalysis products to estimate daily weather variables in a hot summer mediterranean climate. Agronomy 11(6):1207
Saha S, Moorthi S, Pan HL, Wu X, Wang J, Nadiga S, Tripp P, Kistler R, Woollen J, Behringer D, Liu H (2010) NCEP climate forecast system reanalysis (CFSR) 6-hourly products, January 1979 to December 2010. Research Data Archive at the National Center for Atmospheric Research, Computational and Information Systems Laboratory, Boulder, CO. https://doi.org/10.5065/D69K487J. Accessed on 05-May-2021
Saha S, Moorthi S, Wu X, Wang J, Nadiga S, Tripp P, Behringer D, Hou Y, Chuang H, Iredell M, Ek M (2011) updated daily. NCEP climate forecast system version 2 (CFSv2) 6-hourly products, research data archive at the National Center for Atmospheric Research, Computational and Information Systems Laboratory. https://doi.org/10.5065/D61C1TXF. Accessed on 05-May-2021
Singh AK, Goyal V, Mishra AK, Parihar SS (2013) Validation of CropSyst simulation model for direct seeded rice-wheat cropping system. Curr Sci 104(10)
Sun W, Mu X, Song X, Wu D, Cheng A, Qiu B (2016) Changes in extreme temperature and precipitation events in the Loess Plateau (China) during 1960–2013 under global warming. Atmos Res 168:33–48
Wang X, Jiang D, Lang X (2017) Future extreme climate changes linked to global warming intensity. Sci Bull 62(24):1673–1680
Willmott CJ (1981) On the validation of models. Phys Geogr 2:184–194
Willmott CJ, Matsuura K (2005) Advantages of the mean absolute error (MAE) over the root mean square error (RMSE) in assessing average model performance. Climate Res 30(1):79–82
Yue S, Wang CY (2002) Applicability of prewhitening to eliminate the influence of serial correlation on the Mann-Kendall test. Water Resour Res 38(6):4–1
Zhang G, Su X, Ayantobo OO, Feng K, Guo J (2020) Remote-sensing precipitation and temperature evaluation using soil and water assessment tool with multiobjective calibration in the Shiyang River Basin, Northwest China. J Hydrol 590:125416
Zhao S, Zhou T, Chen X (2020) Consistency of extreme temperature changes in China under a historical half-degree warming increment across different reanalysis and observational datasets. Clim Dyn 54(3):2465–2479
Zhou J, Huang J, Zhao X, Lei L, Shi W, Wang L, Wei W, Liu C, Zhu G, Yang X (2020) Changes of extreme temperature and its influencing factors in Shiyang river basin, northwest China. Atmosphere 11(11):1171
Zittis G, Hadjinicolaou P, Fnais M, Lelieveld J (2016) Projected changes in heat wave characteristics in the eastern Mediterranean and the Middle East. Reg Environ Chang 16:1863–1876